Supplementary Figure 1
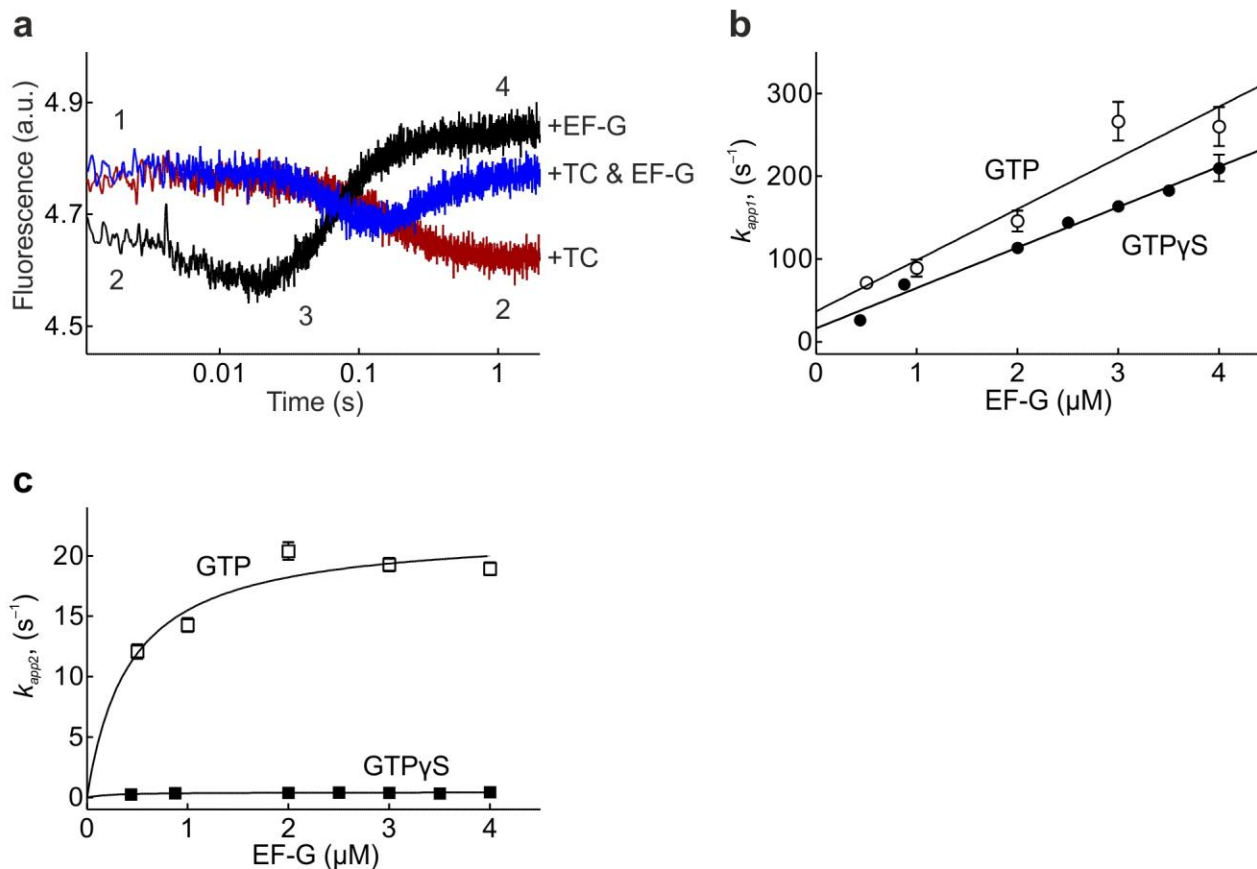
Functional activity of fluorescence-labeled ribosome complexes used in this study, as determined by the time-resolved puromycin assay.

Closed circles, unlabeled PRE complex; open circles, S13-Alx; closed squares, S13-Q–L33-Alx; open squares, S6-Alx488–L9-Alx568, triangles, tRNA(Flu)–L33-Q. The full activity of the PRE L12-Alx–EF-G-QSY9 complexes was reported earlier[30].

Supplementary Figure 2

Translocation as monitored by fluorescence changes of S13-Alx.

(**a**) Fluorescence changes of S13-Alx accompanying PRE and POST complex formation. Addition of the ternary complex EF-Tu–GTP–Phe-tRNA[Phe] (TC) to the initiation complex 70S–mRNA–fMet-tRNA[fMet] (IC) leads to the formation of the PRE complex (1→2, dark red); EF-G–GTP is added to the PRE complex, forming the POST complex (2 → 3 → 4, black); TC and EF-G–GTP together are added to IC (1 → 4, dark blue). (**b**) Linear dependence of k_{app1} from the exponential fitting of time courses; slopes are 62 ± 10 $\mu M^{-1} s^{-1}$ (GTP) and 49 ± 2 $\mu M^{-1} s^{-1}$ (GTPγS). (**c**) In the presence of GTP the hyperbolic fit of k_{app2} saturates at 22 ± 2 s^{-1} with an apparent K_M of 0.4 ± 0.2 μM; the k_{app3} value is 1 s^{-1} independent of EF-G concentration (data not shown). With GTPγS, k_{app2} saturates at a rate of 0.43 ± 0.02 s^{-1} with an apparent K_M of 0.2 ± 0.1 μM; k_{app3} was not observed. The rate of GTPγS hydrolysis is about 0.005 s^{-1} at 37°C (ref. 9). Values are mean and s.e.m. of the fit (n = 8 technical replicates). In those cases where the error bars are not seen, the value is smaller than the symbol size.
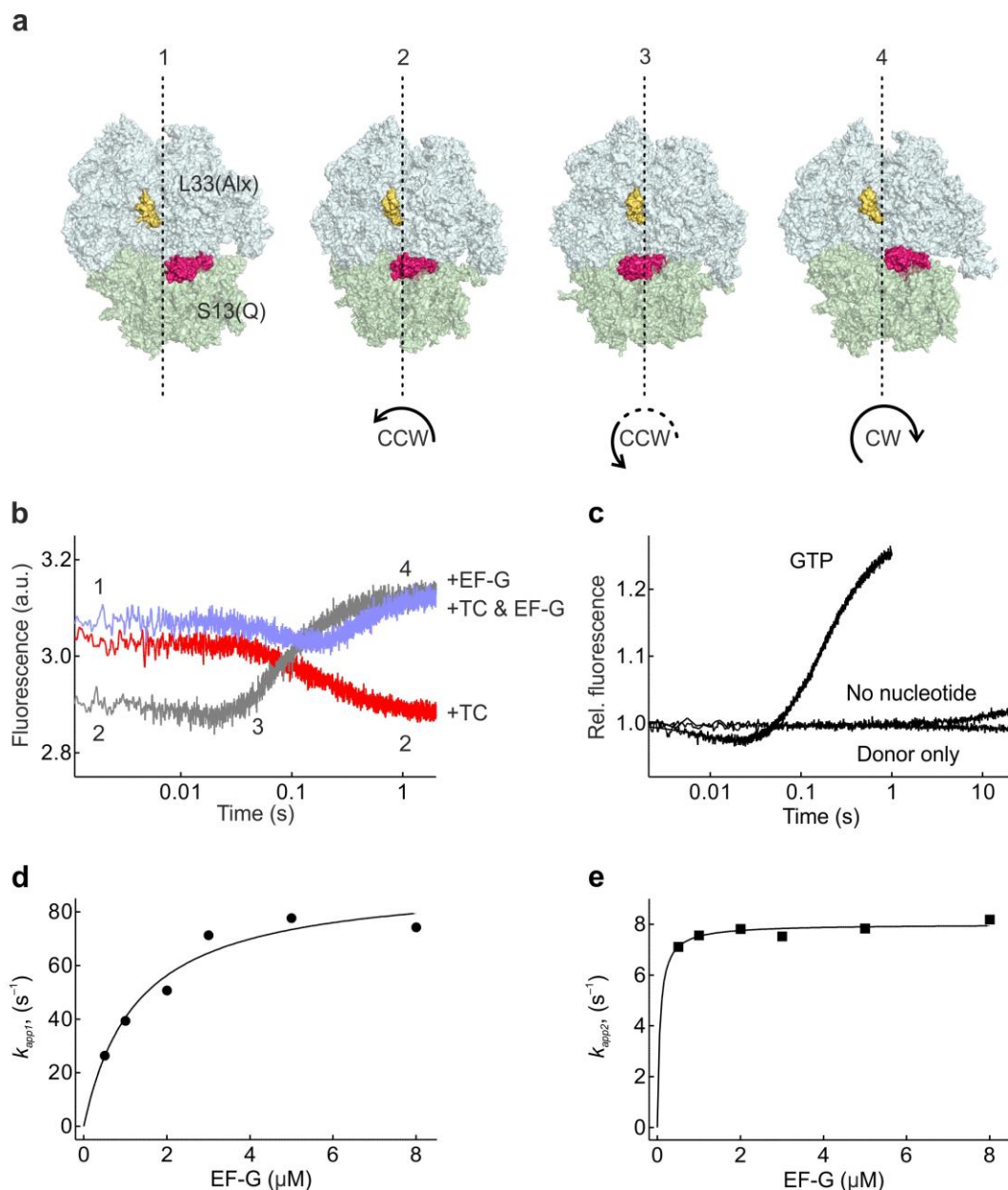
Supplementary Figure 3

Controls for SSU head dynamics monitored by S13-L33 FRET.

(**a**) Ribosome intermediates describing the rotational movements of the SSU head during the transition from PRE to POST states[10, 23, 24] (Schuwirth, B.S. et al. *Nat. Struct. Mol. Biol.* **13**, 879-86 (2006); Borovinskaya, M.A. et al. *Nat. Struct. Mol. Biol.* **14**, 727-32 (2007), Dunkle, J.A. et al. *Science* **332**, 981-4 (2011)). Protein S13, magenta; L33, yellow. (**b**) FRET changes upon addition of the ternary complex EF-Tu–GTP–Phe-tRNA^{Phe} (TC) to the initiation complex 70S–mRNA–fMet-tRNA^{fMet} (IC) leads to the formation of the PRE complex (1→2, red); EF-G–GTP was added to the PRE complex, forming the POST complex (2 → 3 → 4, gray); TC and EF-G–GTP together are added to IC (1 → 4, light blue). (**c**) Translocation reactions were carried out with EF-G and double-labeled PRE complex (S13-Q–L33-Alx) or single-labeled PRE complex (L33-Alx) (donor only) in the presence or absence of GTP. PRE complexes were mixed with EF-G with or without GTP (Methods). (**d**) The hyperbolic fit of k_{app1} saturates at 92 ± 7 s^{-1} with an apparent K_M = 1.2 ± 0.3 μM. (**e**) The k_{app2} value saturates at 8.1 ± 0.1 s^{-1}, K_M = 0.06 ± 0.02 μM. Values are mean and s.e.m. of the fit (*n* = 8 technical replicates); s.e.m. values are smaller than the symbol size. Anisotropy of the Alexa488 dye attached to L33 on the ribosome is 0.159 ± 0.002, which is sufficiently low to consider the ‹κ^2› = 2/3 a valid approximation[44].
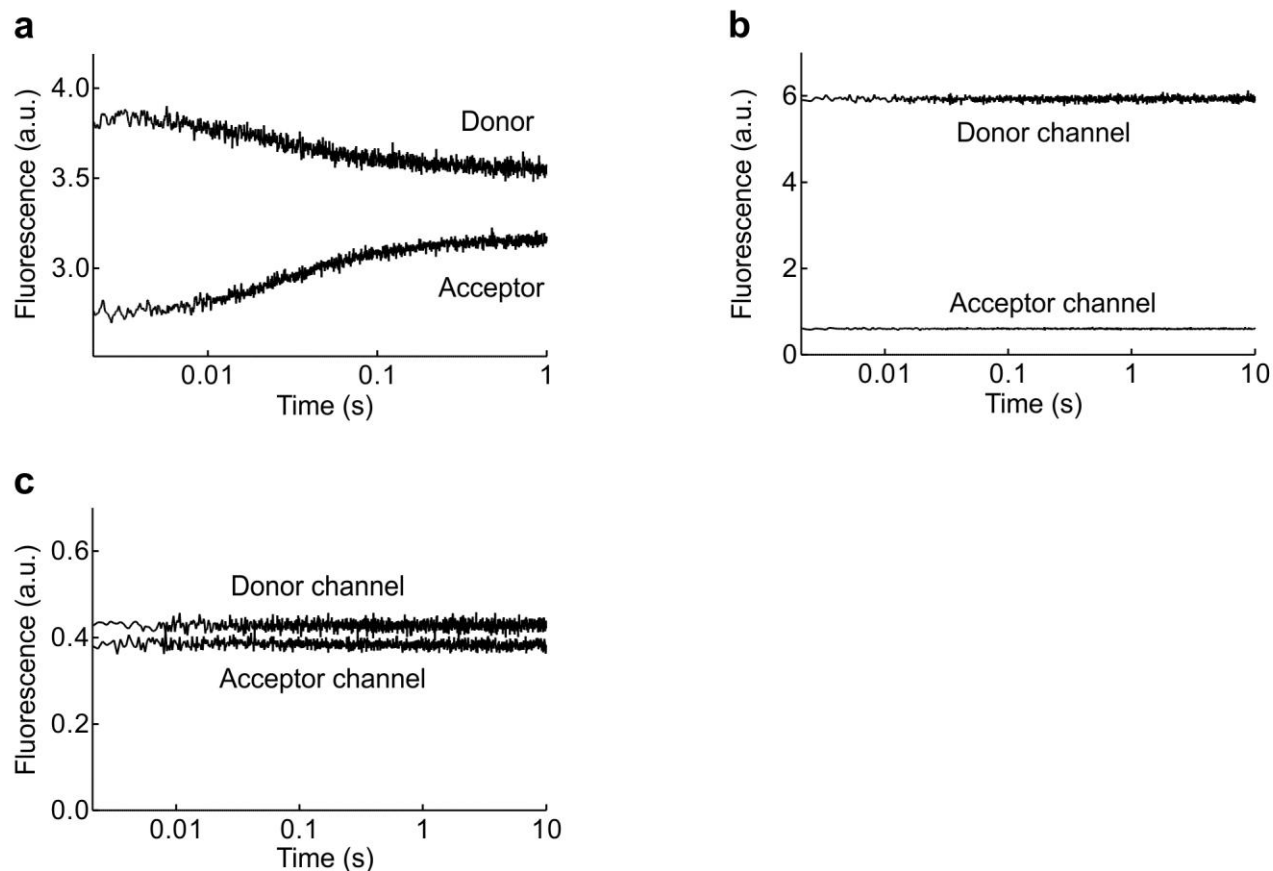
Supplementary Figure 4

Controls for SSU-LSU rotation monitored by S6-L9 FRET.

(**a**) FRET change upon mixing EF-G–GTP with PRE complexes (S6-Alx488) and L9-Alx568) monitored in donor and acceptor channels. The decrease in donor fluorescence is attenuated by an increase in acceptor fluorescence, due to the use of a cut-off filter. (**b**) Fluorescence in donor and acceptor channels monitored with single-labeled S6-Alx488 ribosomes. (**c**) Fluorescence in donor and acceptor channels monitored with single-labeled L9-Alx568 ribosomes. Anisotropies of the Alexa488 on S6 and Alexa568 on L9 in single-labeled 70S ribosomes are 0.197 ± 0.003 and 0.292 ± 0.002, respectively. Despite the relatively high anisotropy of the acceptor dye, the FRET efficiency is not affected by the dye orientation[25, 44]. Other spectroscopic properties of the FRET pair are described elsewhere[25].
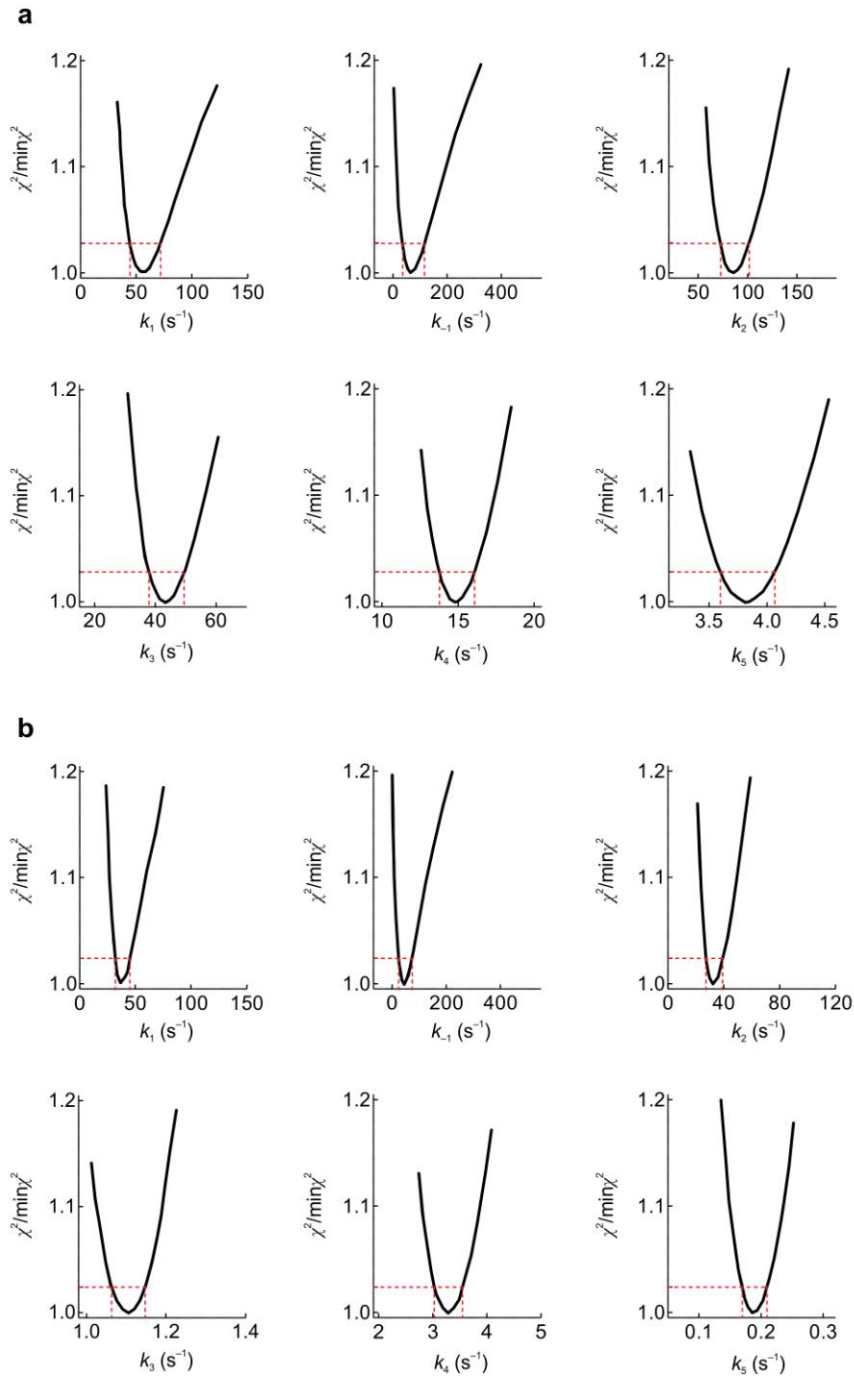
Supplementary Figure 5

Goodness of global fitting for a five-step reaction model.

Analysis of the confidence contour based on the search for SSE (Sum of Square Error) minima while varying one parameter (i.e. rate constant) at a time[31]. The sharpness of the minimum peaks denotes an optimal resolution of all rate constants describing the EF-G–dependent translocation in the presence of GTP (**a**) and GTPγS (**b**). Red dashed lines show the lower and upper boundaries as calculated for a χ^2 threshold of 1.025 (refs. 31,45,46).
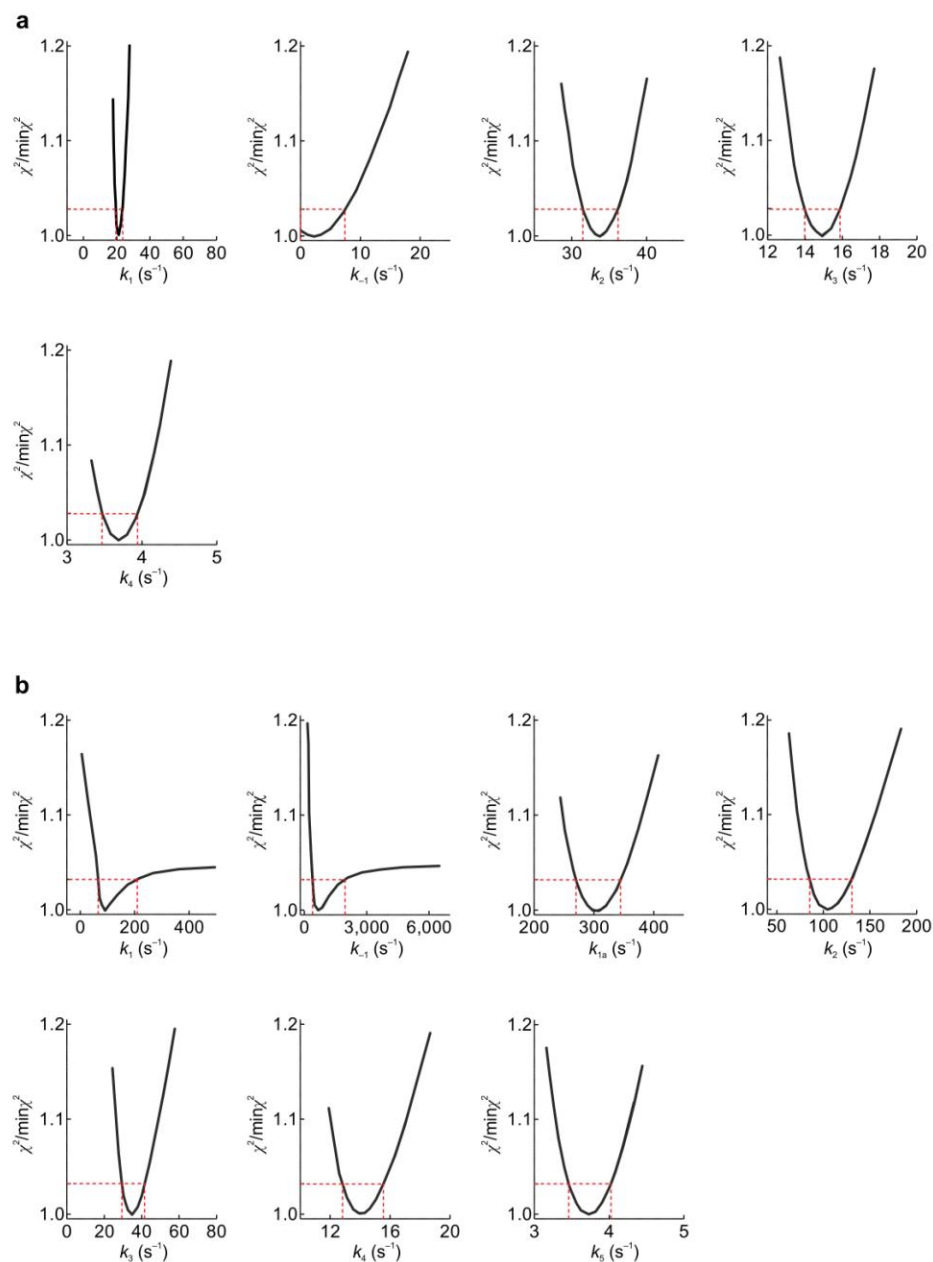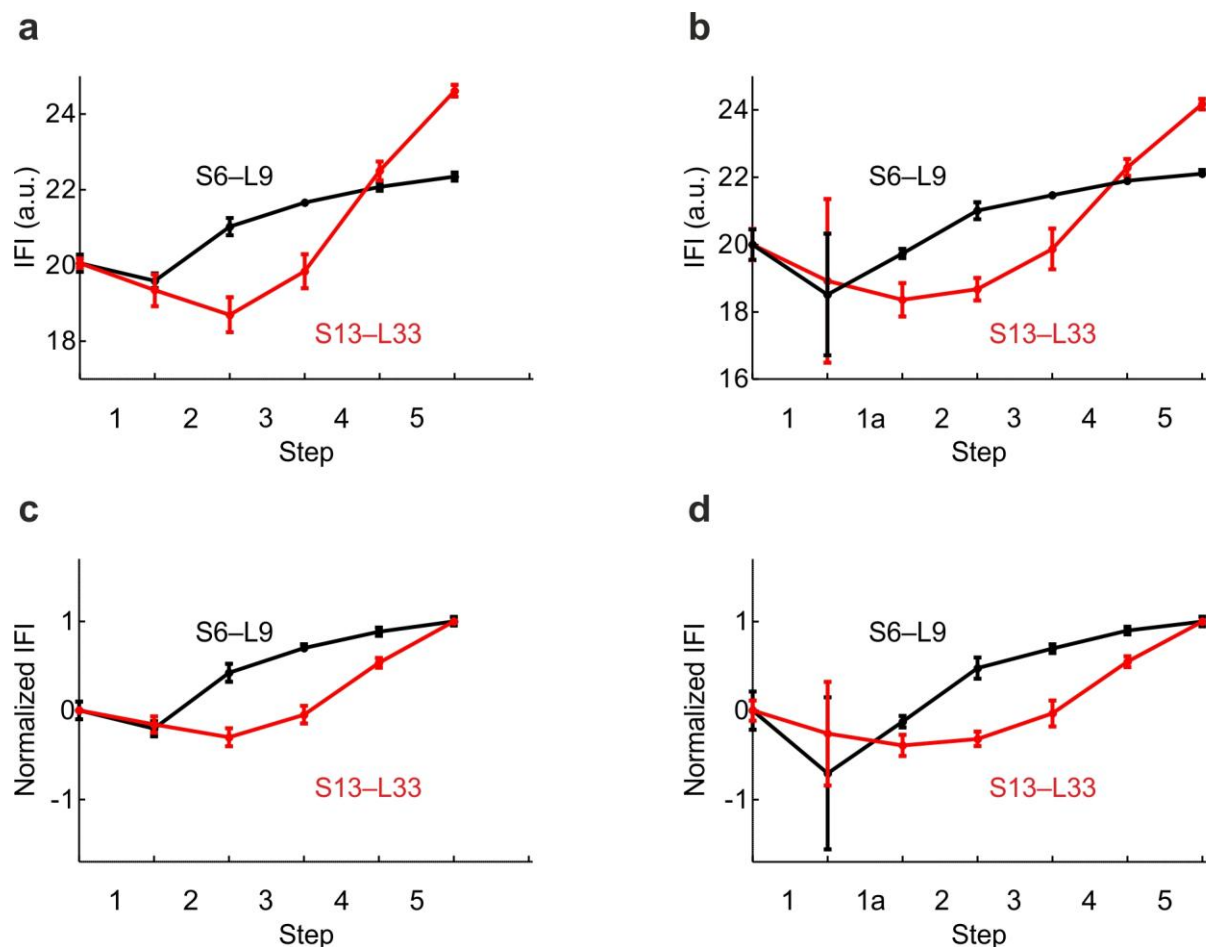
Supplementary Figure 6

Goodness of global fitting for four-step and six-step reaction models.

(**a**) For the four-step scheme, the lower limit for k_{-1} is undefined, the estimated k_1 is much lower than estimated from the concentration dependence of k_1 in Supplementary Fig. 2b, and a monomolecular step of about 100 s^{-1} corresponding to GTP hydrolysis[19, 33] is not defined. Visual inspection indicates deviations of the fit to the four-step model from the experimental data (not shown), suggesting that global fitting to a four-step scheme does not provide a consistent fit.

(**b**) For the six-step scheme, the upper limits for k_1 and k_{-1} are poorly defined; the rate of additional step 1a is about 300 s^{-1}, which is not observed directly, but cannot be excluded. Regardless of the model, global analysis robustly finds three steps, with the global minima at about 33-43 s^{-1}, 14-15 s^{-1}, and 4 s^{-1}, corresponding to steps 3, 4, and 5 of the five-step model; step 2 with the rate of 80-100 s^{-1} is well-defined in the five- and six-step models and consistent with the previous data. Red dashed lines show the lower and upper boundaries as calculated for a χ^2 threshold of 1.025 for the four-step model (the calculated χ^2 threshold of the fit is 1.0025) and 1.032 for the six-step model (the calculated χ^2 threshold of the fit is 1.0032) (refs. 31,45,46).

Supplementary Figure 7

Comparison of the IFI values for the five-step and six-step models.

(**a,b**) Absolute IFI values for the S13-L33 (red) and S6-L9 (black) FRET pairs. (**c,d**) Normalized representation of the same data. Note that the trend for the IFI changes is independent of the model. The only difference is the presence of an additional, very rapid step (step 1a or k_{1a} = 300 s^{-1}) in the six-step model (Supplementary Fig. 6b), for which the global fit does not give a statistically significant solution. Average IFI values and error bars are averages with error bars representing standard deviations (s.d.) (n = 3 independent kinetic experiments); in comparison, the s.e.m. of the fit for each IFI is smaller than the symbol size (not shown).
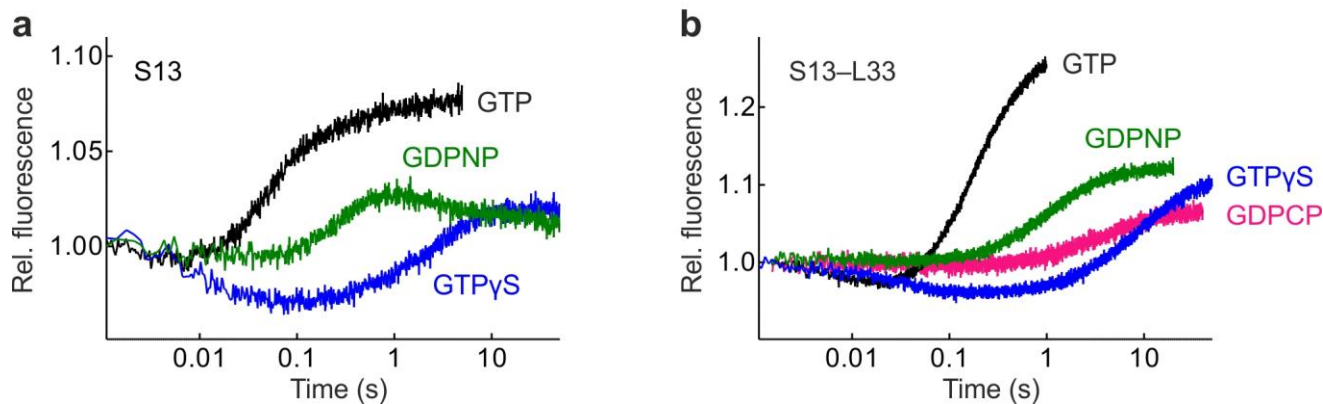
Supplementary Figure 8

EF-G–catalyzed translocation with GTP and nonhydrolyzable GTP analogs.

(a) S13 fluorescence. The final fluorescence is very similar for GTPγS (blue) and GDPNP (green) and much higher when GTP (black) is used and hydrolyzed by EF-G, suggesting a different final conformation of the complex, probably due to the retention of EF-G. The overall shape of the time course obtained with GDPNP differs from that monitored with GTP. (b) S13-L33 FRET. The final level is similar for all three non-hydrolysable analogs and lower than after GTP hydrolysis. The apparent rates of the upward reaction range between 0.1 s^{-1} (GTPγS), 0.2 s^{-1} (GDPCP, pink) and 0.7 s^{-1} (GDPNP) compared to 8 s^{-1} (GTP, cf. Supplementary Fig. 3e). Note that in **a** and **b** the downward phase (reflecting steps 1 and 2, respectively) is kinetically similar with GTP and GTPγS (see also Fig. 6), but is not observed with GDPNP and GDPCP.